DOI 10.1007/s10443-016-9508-1

Finite Element Simulation of Low Velocity Impact Damage on an Aeronautical Carbon Composite Structure

Roger Pierre Lemanle Sanga[1] · Christian Garnier[1] · Olivier Pantalé[1]

Abstract Low velocity barely visible impact damage (BVID) in laminated carbon composite structures has a major importance for aeronautical industries. This contribution leads with the development of finite element models to simulate the initiation and the propagation of internal damage inside a carbon composite structure due by a low velocity impact. Composite plates made from liquid resin infusion process (LRI) have been subjected to low energy impacts (around 25 J) using a drop weight machine. In the experimental procedure, the internal damage is evaluated using an infrared thermographic camera while the indentation depth of the face is measured by optical measurement technique. In a first time we developed a robust model using homogenised shells based on degenerated tri-dimensional brick elements and in a second time we decided to modelize the whole stacking sequence of homogeneous layers and cohesive interlaminar interfaces in order to compare and validate the obtained results. Both layer and interface damage initiation and propagation models based on the Hashin and the Benzeggagh-Kenane criteria have been used for the numerical simulations. Comparison of numerical results and experiments has shown the accuracy of the proposed models.

Keywords Composite structure · Impact · Damage · Finite element method · BVID

1 Introduction

Modern aerospace structures are using more and more composite materials because of their high specific mechanical properties (strength and stiffness) with regard to their specific weight mass. However, resistance of those structures in case of external solicitations such as

✉ Olivier Pantalé
pantale@enit.fr

[1] INP de Toulouse, ENI de Tarbes, Laboratoire Génie de Production, Université de Toulouse, avenue d'Azereix, B.P. 1629, 65016 Tarbes, France

low velocity impacts can drastically reduce their mechanical properties, particularly in the case of thermoset matrix like the epoxy. Aeronautical structures are subjected during their lifetime to various impacts resulting of aleas such as dropped tools, handling accidents or hail impacts. Knowledge about damage initiation and propagation in layered carbon/epoxy structures, usually called Barely Visible Impact Damage (BVID) is therefore a major subject of interest for many years in aerospace industry. Such internal damage lead to significant reduction of the local strengths: matrix cracking [1], splitting between fibres or internal delamination in case of bending stresses as reported by Abrate [2, 3]. The major problem is that this damage can be completely invisible when viewed from the external surface of the involved structure. It is therefore very important to detect this kind of damage and to be able to predict damage initiation and propagation using various techniques in order to predict the real residual lifetime of a structure under dynamic solicitations. The large number of publications available nowadays is an evidence of the interest of industrials and academics concerning this topic for many years.

In the first section of this paper, we present the BVID experiment and the experimental results obtained on the MTT drop weight machine. The first part concerns the presentation of the material and specimens, the second part the presentation of the experimental device and measuring techniques, and the last part the experimental results. The second section is dedicated to the presentation of the Finite Element Modelling of the BVID impact test. The first part is dedicated to the presentation of the damage models and the propagation criteria for the both parts: the layer and the interfacial part. Two different simulation models are then presented: the first one is based on the use of homogenised conventional shell elements with a reduced integration scheme while the second one models the whole stacking sequence of layers. A comparison and validation of both approaches is presented at the end of this section.

2 BVID Experiments and Results

BVID defaults resulting from low velocity impacts are the hidden menace for composite materials mainly because the resulting damage is not visible on the surface of the specimen. The aerospace industry uses laboratory drop weight machines to impact coupon size composite specimens and measure damage resulting from such experiments. Residual compressive strength measures of the coupon after impact usually done by a Compression After Impact test (CAI) is one of the major approach used to give an idea of the internal damage of the composite. Over the last twenty years, Non Destructive Testing (NTD) such as the Ultrasonic testing [4] or the Infrared Thermography [5–7] has been used to evaluate the internal damage resulting from a BVID.

They are many definition of low velocity or low energy impact due of the great number of parameters that should be study such as the velocity, the shape and the mass of the impactor [8]. For Olsson [9], when the impact response is influenced by shear and flexural wave from boundary condition, this phenomenon is classified as low velocity impact. Sjöblom et al. [10] and Shivakumar et al. [11] have defined that the low energy impact can be considered as a quasi-static solicitation. According to those authors, the upper limit of the low velocity impact speed ranges from 1 to 10 m/s depending on the stiffness and the material of the impacted plate and on the mass of the impactor. The dynamical response of the structure depends therefore on the duration of the contact between the structure and the impactor. Cantwell and Morton [12] have proposed that every dynamic solicitation corresponding to an impact speed below 10 m/s to 20 m/s can be considered as a low velocity impact. On the

other hand, Abrate [2] considers that the impact speed limit defining a low velocity impact is five to ten time greater than the one proposed by Cantwell and Morton (100 m/s). Liu et al. [13] and Joshi [14] are using a different approach based on the internal damage of the impacted structure. They postulate that a high velocity impact leads to fibres rupture whereas low velocity impact leads to internal delamination and matrix cracking. Cesari et al. [15] have analysed the influence of the impact on the residual strength limit using CAI tests. During their work, they studied the defaults generated by the impact and have shown the existence of a limit for the detection of those defaults by visual inspection. The kind of default generated at this limit, is so called the Barely Visible Impact Damage (BVID). In our case, the BVID is characterized by a small indentation of the front face of the specimen in the impact zone, around 0.3 mm, some matrix cracks and delamination and some fibres breakage or fibres splitting at the back face of the specimen.

2.1 Material and Specimens

The material used in this work is a carbon epoxy composite produced by the Liquid Resin Infusion process. A woven Satin 5 pattern called HexForce G0926® made from carbon fibers Tenax HTA40 combined to the HexFlow RTM6® epoxy thermoset resin has been selected for this application. The weight distribution of the carbon fabric is 50 % on both the warp and the weft directions and the nominal weight is 370 g/m^2.

The lay-up of the specimen is $[[0°/45°]_3]_s$ for a total thickness of 4.44 mm. All specimens were controlled after production to ensure that the average rate of porosity is under 2.5 % in volume. The plate's dimensions are 150×100 mm^2. All mechanical properties of the composite, carried out from tensile tests and ultrasonic measurements realized in a previous study, are reported in Table 1.

2.2 Testing Device and Results

The specimens under investigation were damaged by a low velocity impact. The experimental device is composed of a MTT (Material Testing Technology) drop weight machine with a maximal capacity of 60 J as illustrated in Fig. 1. The impactor is a $\phi = 16$ mm hemispherical tap with a weight of $m = 3$ kg. The dropping height is $h = 0.85$ m leading to an impact energy of 25 J and an impact speed of $V_i = 4.1$ m/s.

The 25 J impact at the center of the specimen produced barely visible damages on the impacted specimen. In order to relax the major part of the internal stresses inside the matrix, a waiting time of 48 h before measurements have been chosen. The indentation of the front face of the specimen is measured by using optical systems from GOM Software. The Atos/Tritop softwares are used to digitize the central zone of the front face of the impacted specimen with a precision of 0.02 mm. Therefore, an indentation depth of 0.24 mm on the face has been measured. The internal damage is evaluated using an infrared thermographic camera (a FLIR MWIR Titanium camera with a thermal resolution of 20 mK) as presented in Garnier et al. [5]. Halogen lamps placed at 150 mm from the back face of the specimen are used to provide thermal sollicitation of the sample. The specimen is heated for 5 s and a

Table 1 Mechanical properties of the G0926/RTM6 composite

Young modulus	$E_1 = 67.9$ GPa	$E_2 = 67.9$ GPa	$E_3 = 12.1$ GPa
Shear modulus	$G_{12} = 6.2$ GPa	$G_{13} = 4.5$ GPa	$G_{23} = 4.5$ GPa
Poisson ratio	$\nu_{12} = 0.06$	$\nu_{13} = 0.17$	$\nu_{23} = 0.17$

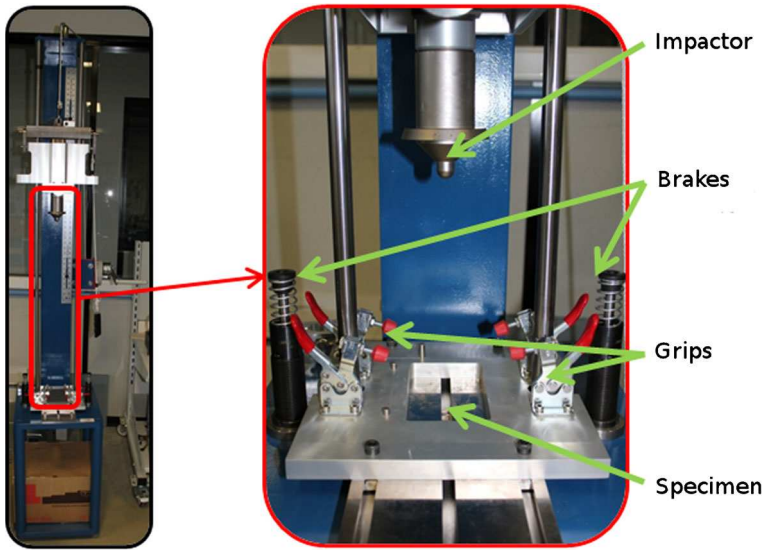

Fig. 1 MTT drop weight machine

30 s movie is recorded with a frame-rate of 152 Hz. The presence of the defect appears during heating and cooling time and the output of this procedure is the projection of the internal default on a 2D plane as illustrated in Fig. 2. The measured surface of the defect is 449 mm^2.

3 Finite Element Modeling of BVID

Numerical simulation of composite materials has been developed since the 80's. Simulation of composite structures is based on a mesoscopic scale, i.e. in between the microscopic one corresponding to the base components of the material and the macroscopic scale corresponding to the global approach. The composite structure is therefore decomposed into a stacking sequence of homogeneous layers and cohesive interlaminar interfaces. Damage initiation and propagation criteria of both layers and cohesive interfaces are presented here after.

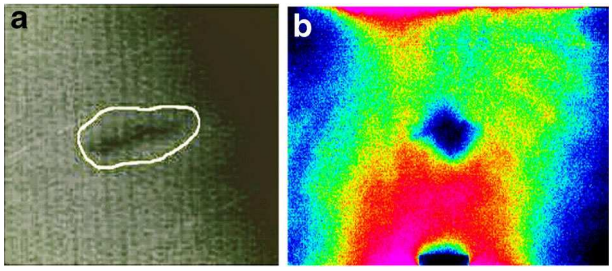

Fig. 2 Impact damage visualization using x-ray tomographic (**a**) and infrared camera (**b**)

3.1 Damage Models and Criteria

Cohesive interlanimar interfaces are used to transfer stress and strains from one layer to the next one inside the stacking sequence. They are introduced to modelize the separation of the consecutive layers thanks to a damage criterion as proposed by Allix et al. [16]. In the following formulations, $\hat{\sigma}_{ij}$ will denote the effective stress, exponents $()^t$ and $()^c$ denote traction and compression respectively and indices $()_f$ and $()_m$ are used to refer fiber and matrice respectively.

3.1.1 Layer Damage Model

Many damage theories have been developed in the last past years. Most of these approaches are based on the works of Kachanov and Rabotnov [17, 18]. In commercial finite element codes the material is considered to be initialy undamaged and to follow an isotropic or orthotropic elastic behavior. As the stress increases in the structure, depending on the damage criterion, the initiation of the damage occurs. Therefore, the behaviour of the material is changed and a damage evolution criterion is added to the material behaviour and increases upto the final erosion of the element. The Hashin [19] criterion is widely used and considers four different damage initiation mechanisms as described here after. The initiation criteria have the following general forms:

– fibre tension $\widehat{\sigma}_{11} \geq 0$:

$$F_f^t = \left(\frac{\widehat{\sigma}_{11}}{X^t}\right)^2 + \alpha \left(\frac{\widehat{\sigma}_{12}}{S^l}\right)^2 \tag{1}$$

– fibre compression $\widehat{\sigma}_{11} < 0$:

$$F_f^c = \left(\frac{\widehat{\sigma}_{11}}{X^c}\right)^2 \tag{2}$$

– matrix tension $\widehat{\sigma}_{22} \geq 0$:

$$F_m^t = \left(\frac{\widehat{\sigma}_{22}}{Y^t}\right)^2 + \left(\frac{\widehat{\sigma}_{12}}{S^l}\right)^2 \tag{3}$$

– and matrix compression $\widehat{\sigma}_{22} < 0$:

$$F_m^c = \left(\frac{\widehat{\sigma}_{22}}{2S^t}\right)^2 + \frac{\widehat{\sigma}_{22}}{Y^c}\left[\left(\frac{Y^c}{2S^t}\right)^2 - 1\right] + \left(\frac{\widehat{\sigma}_{12}}{S^l}\right)^2 \tag{4}$$

In the previous equations, X^t and X^c are the tensile and compressive strength in fiber direction, Y^t and Y^c are the tensile and compressive strength in transverse direction, S^l and S^t are the longitudinal and transverse shear strength respectively and α is a coefficient that determines the contribution of the shear stress to the fiber tensile initiation criterion. This later can be used to select the Hashin [19] model ($\alpha = 1$) or the Hashin and Rotem [20] model ($\alpha = 0$ and $S^t = \frac{Y^c}{2}$). The components of the effective stress tensor: $\widehat{\sigma}_{11}$ (stress in the fiber direction), $\widehat{\sigma}_{22}$ (stress in the transverse-to-the fiber direction) and $\widehat{\sigma}_{12}$ (in-plane shear stress) are evaluated through the following relation:

$$\hat{\sigma} = \begin{bmatrix} \frac{1}{1-d_f} & 0 & 0 \\ 0 & \frac{1}{1-d_m} & 0 \\ 0 & 0 & \frac{1}{1-d_s} \end{bmatrix} \sigma \tag{5}$$

where σ is the true stress and d_f, d_m and d_s are internal damage variables that characterize fiber, matrix and shear damage which are defined from the damage variables d_f^t, d_f^c, d_m^t and d_m^c by:

$$d_f = \begin{cases} d_f^t & \text{if } \widehat{\sigma}_{11} \geq 0 \\ d_f^c & \text{if } \widehat{\sigma}_{11} < 0 \end{cases} \tag{6}$$

$$d_m = \begin{cases} d_m^t & \text{if } \widehat{\sigma}_{22} \geq 0 \\ d_m^c & \text{if } \widehat{\sigma}_{22} < 0 \end{cases} \tag{7}$$

$$d_s = 1 - \left(1 - d_f^t\right)\left(1 - d_f^c\right)\left(1 - d_m^t\right)\left(1 - d_m^c\right) \tag{8}$$

Prior to any damage initiation and evolution inside the material, the initial conditions associated to the problem are the following ones:

$$d_m^t = d_m^c = d_f^t = d_f^c = 0$$

An interfacial damage model, able to describe the mechanical behavior of the interfaces has to be included in the structural model. Usually, this kind of damage model is based on the use of cohesive elements, cohesive surfaces or springs as proposed for example by Camanho et al. [21]. Cohesive elements and cohesive surfaces are widely used to model the adhesive structure between two layers. Cohesive elements are well adapted to modelize glue joints while cohesive surfaces with a zero thickness are well adapted for delamination problems. The mechanical behaviour presents two phases: the initiation on the one hand and the propagation on the other hand.

3.1.2 Interface Damage Model

Initiation Criterion The initiation criterion is usually based on the measure of stresses or strains. In the proposed approach, damage is assumed to initiate when a quadratic interaction function involving the nominal stress ratios (as defined in the expression below) reaches a value of one. This criterion can be represented as:

$$\left(\frac{\langle \sigma_n \rangle}{N_{max}}\right)^2 + \left(\frac{\sigma_t}{T_{max}}\right)^2 + \left(\frac{\sigma_s}{S_{max}}\right)^2 = 1$$

where $\langle\rangle$ represents the Macaulay bracket (in this application:$\langle \sigma_n \rangle = \frac{1}{2}\left(|\sigma_n| + \sigma_n\right)$) with the usual interpretation, σ_n is the normal nominal strain, σ_s and σ_t are the first and second shear directions. The Macaulay brackets are used to signify that a pure compressive deformation or stress state does not initiate damage.

Propagation Criterion Propagation criterion are used to describe the rate at which the material stiffness is degraded once the corresponding initiation criterion defined above is reached. Major part of those damage criterion are based on an energy criterion with a fuction of mode mix using either a tabular form or an analytical form. Jäger et al. [22] recently present a new finite element model to predict damage mechanism in laminate composite plates subjected to mode I, mode II and low velocity transverse impact where they use a power law analytical form of the energy-based damage evolution. In our case we decided to use the Benzeggagh-Kenane analytical form. We usually denote by G_n, G_s and G_t the work done by the tractions and their conjugate relative displacements in the normal, first, and second shear directions, respectively. The Benzeggagh-Kenane fracture criterion [23] is

particularly useful when the critical fracture energies during deformation purely along the first and the second shear directions are the same. It is given by:

$$G_n^c + \left(G_s^c - G_n^c\right)\left(\frac{G_S}{G_T}\right)^{\eta} = G^c$$

with $G_S = G_s + G_t$ and $G_T = G_n + G_S$, and η is a material parameter.

3.2 Numerical Simulation of BVID

Material properties and geometry of the specimen have already been presented in Section 2.1. The Hashin [20] damage criterion has been selected for our models as this one is already implemented in the Abaqus Explicit [24] FEM code used for the simulations. All the necessary material parameters concerning this damage criterion for the G0926/RTM6 composite are reported in Table 2.

Numerical models involve an explicit integration scheme to simulate the impact for a total time period of 3.5 ms. This duration covers the whole impact problem. In our work we have decided to use two different approaches. In a first time we developed a robust model using homogeneized shells based on degenerated tri-dimensional brick elements. In a second time we decided to modelize the whole stacking sequence of homogeneous layers and cohesive interlaminar interfaces. Both models have been compared and validated concerning their performance and accuracy with regard to the experiments presented earlier in this paper.

As illustrated in Fig. 3, the same kind of boundary conditions have been used for the two models: a restriction of the displacements $u_1 = u_2 = u_3 = 0$ for all nodes located along the lateral edges of the specimen in contact with the fixture base of the MTT drop weight machine. For this part of the specimen ($Zone\,1$), we choose the size of the elements to be $5 \times 5\,\text{mm}^2$. The second partition ($Zone\,2$) of the specimen ($62.5 \times 37.5\,\text{mm}^2$) has an element size of $2 \times 2\,\text{mm}^2$ and the centre one ($Zone\,3$, $25 \times 25\,\text{mm}^2$) has an element size of $1 \times 1\,\text{mm}^2$. The impactor is modeled by an analytical rigid surface associated with a concentrated 3 kg additional mass and the impact velocity has been set to $V_i = 4.1$ m/s for the impactor.

3.2.1 Structural Model

The first model developed in this study is based on the use of the Abaqus [24] Layup model with the S4R conventional shell element. This one is a 4 nodes quadrilateral conventional shell element with a reduced integration scheme (mandatory for an explicit integration scheme).

In order to see if the total energy of the system is constant during the computation, Fig. 4 reports the energies variation during the impact for the structural model. From this later we can see that the total energy (Kinetic Energy + Internal Energy + Hourglass Energy: $E^k + E^i + E^h$) is quasi constant during the impact with a value arround 25 J (i.e. the nominal

Table 2 Hashin damage criterion parameters

Label	Variable	Stress (MPa)
Traction	$X^t = Y^t$	785
Compression	$X^c = Y^c$	612
Longitudinal shear	S^l	70
Transversal shear	S^t	55

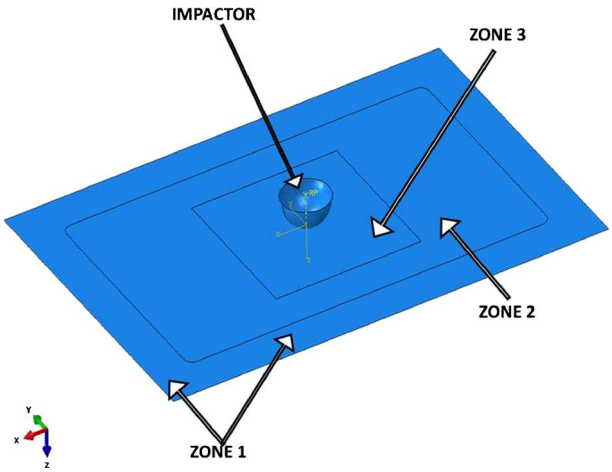

Fig. 3 3D view of the numerical model

BVID energy). Figure 4 shows that the maximum deflection $z_{max} = 2.86\,\text{mm}$ is obtained for $t_m = 1.13\,\text{ms}$. We can see also that the artificial strain energy (Hourglass Energy) E^h associated with constraints used to remove singular modes (hourglass control) remains very low during the impact. More important is the evolution of the energy dissipated by damage (Damage Energy) E^d during the impact. This later has a zero value from the beginning of the impact up-to $t_0 = 0.245\,\text{ms}$. Therefore, at $t_0 = 0.245\,\text{ms}$ the damage initiation criterion is reached and the damage propagation starts. This point corresponds to a divergence of

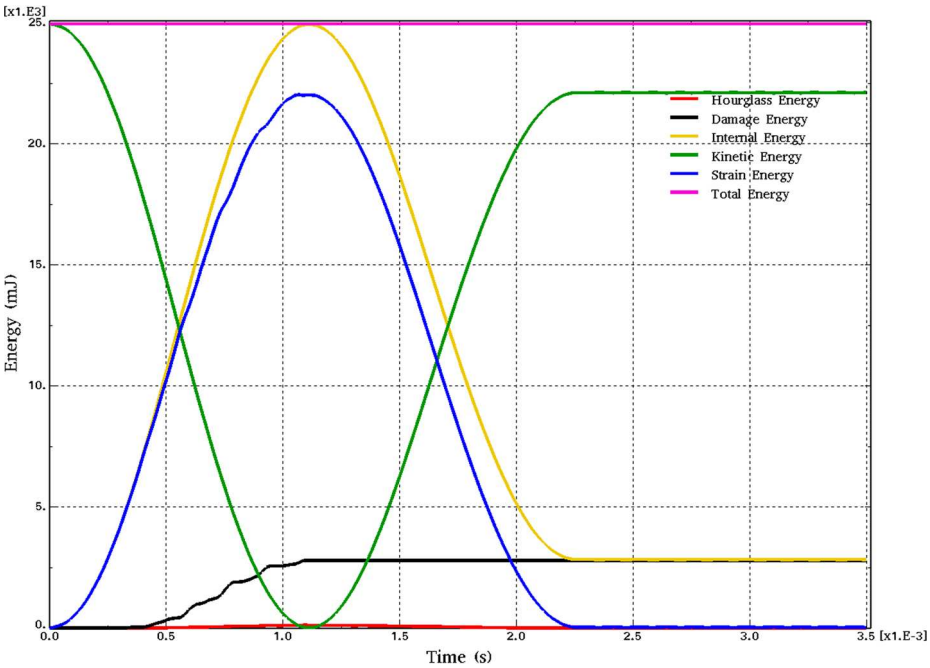

Fig. 4 Energy variation during the impact for the structural model

the recoverable strain energy E^{ε} and the total strain energy (Internal Energy) E^{i} enhancing the fact that: $E^{i} = E^{\varepsilon} + E^{d}$. The damage energy increases up-to $E^{d} = 2.797\,\text{J}$ between $t_0 = 0.245\,\text{ms}$ and $t_1 = 1.12\,\text{ms}$, this period corresponds to the propagation of the damage inside of the structure as a consequence of the impact. Therefore, at $t_1 = 1.12\,\text{ms}$ the damage no longer increases and the final stationnary state has been reached.

The analysis of the Hashin criteria allow to define the most critical damage process after the impact. This analysis has shown that the traction damage d_m^t inside the matrix is the most critical one for the BVID simulation. The explanation comes from the fact that the bottom layers of the specimen are subjected to the major traction strains resulting from the deflexion with regard to the impact, leading to some matrix fissuration due to the fact that this later enhances the lowest mechanical characteristics. Figure 5 shows a contour plot of the traction damage d_m^t inside of the matrix for the structural model at the end of the damage propagation period. In this figure, 454 elements have reached the maximal value for the damage variable and have been removed (white hole in the center of the specimen). As each element represent a surface of $1\,\text{mm}^2$, this leads to a total eroded projected surface of $454\,\text{mm}^2$. This value is very closed to the experimental measures presented in Section 2.2.

3.2.2 Physical Model

The second model developped in this study is a more physical approach, closed to the real build up layer. All 12 layers are modelized and linked one by one with a zero thickness cohesive surface. This kind of approach is more complex than the previous one, mainly because the setup of the model is not automatized and all have been done by hand in this study. A three-dimensional model is therefore constructed and the model includes both the layer and the interfacial damage models presented before. All layers are modelized using Abaqus SC8R continuum shell element. Cohesive surfaces are modelized using the Abaqus COH3D8 element of the standard library.

In this simulation, the total energy of the system is quasi constant during the computation, despite a variation of 2.45 % observed at the maximal deflexion time, as reported in Fig. 6. Also very important, the artificial strain or Hourglass Energy remains very low during the

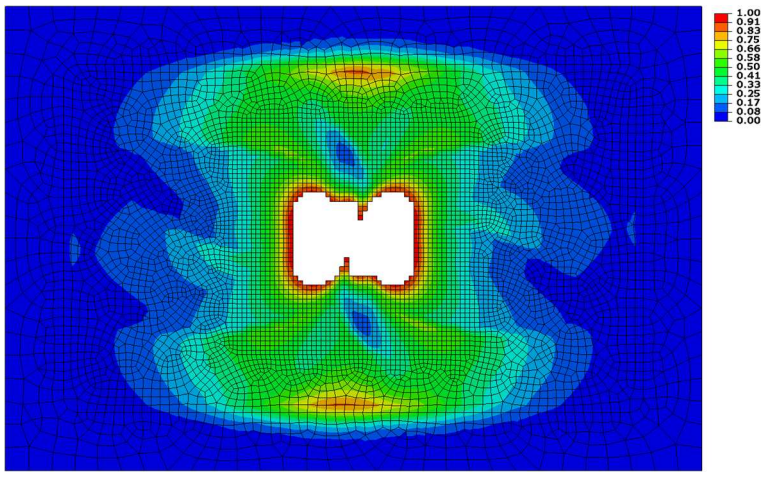

Fig. 5 Final Hashin matrix traction damage d_m^t for the structural model

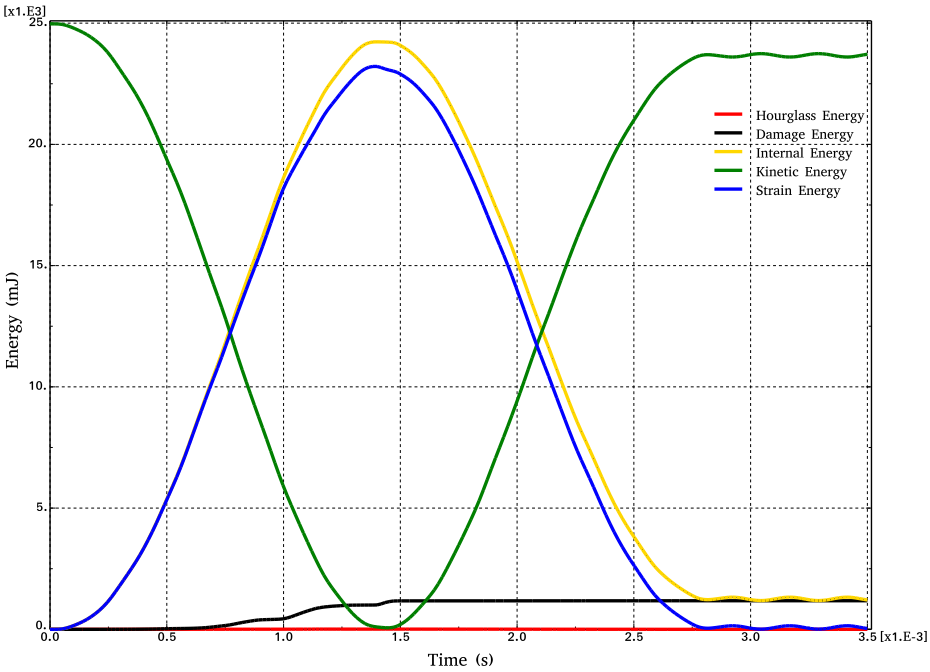

Fig. 6 Energy variation during the impact for the physical model

simulation. Due to the high number of elements involved in the simulation, this second model is more sensitive to hourglass problems, therefore, some artificial strain energy have to be injected during the simulation. As Hourglass Energy is very low compared to the internal energy of the problem (less than 5 % at the end of the simulation [25]), the proposed approach is validated. In Fig. 6, we can see that, the maximal deflection $z_{max} = 3.26\,\text{mm}$ of the specimen is obtained at $t = 1.4\,\text{ms}$, therefore a little bit later than in the previous simulation. At this time, the damage energy increases up-to 1.04 J which is lower than the previous case. This also can be seen by the difference between the Internal Energy and the Strain Energy, during the calculation, which also is greater than in the previous simulation.

As in the previous analysis, Fig. 7 reports the contour plot of the final traction damage for the physical model. In this figure, 332 elements have reached their maximal Hashin matrix traction damage value which represent the surface of $332\,\text{mm}^2$. In Fig. 8 are reported the contour plot of the final delaminated damage for the physical model. The total delaminated elements are 514 which represent the surface of $514\,\text{mm}^2$. To plot the total damaged surface we may combine the two surfaces. We also remark that the first surface of $332\,\text{mm}^2$ is included in the second one. Then, the total projected damaged surface is $514\,\text{mm}^2$. For a better understanding of the situation, Fig. 9 shows a three-dimensional representation of the damaged zone with only the cohesive interfaces represented. The number of erroded elements increases from one layer to another one from the impacted surface up-to the rear surface of the specimen, as usually observed in experimental impacts where the maximum defaults are located near the rear surface of the specimen.

Let's now have a closer focus on the damage energy which results from the addition of the layer damage energy and the cohesive interface damage energy. Figure 10 shows the evolution of the damage energies versus time on each zone which are seriously damaged.

.

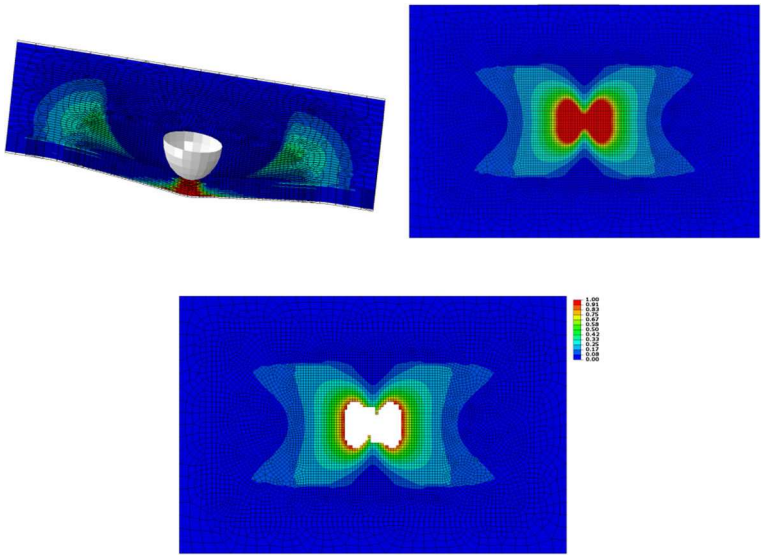

Fig. 7 Final Hashin matix traction damage d_m^t for the structural model

From this later, we can see that each damage energies has the same evolution during the time. Also we see that the damage energy of the cohesive zone $E^d_{Coh} = 1.297\,\text{mJ}$ at the end is lower than the damage energy of layers $E^d_{Plies} = 1.178\,\text{J}$. But as seen earlier, the cohesive zone damaged elements are greater than those of the plies. It means that, the necessary energy to initiate the delamination is smaller than the one to initiate the Hashin matrix-traction damage. This can also be explain by the fact that the proportion of cohesive zone

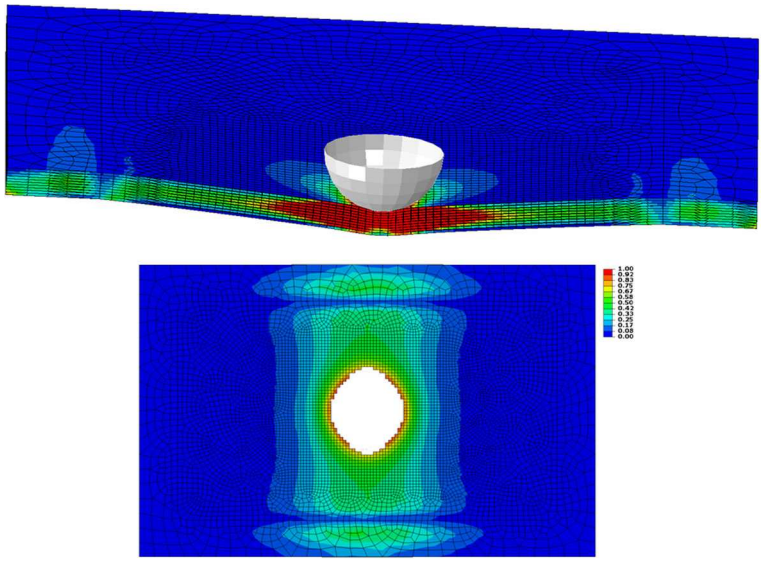

Fig. 8 Final delaminated zone for the structural model

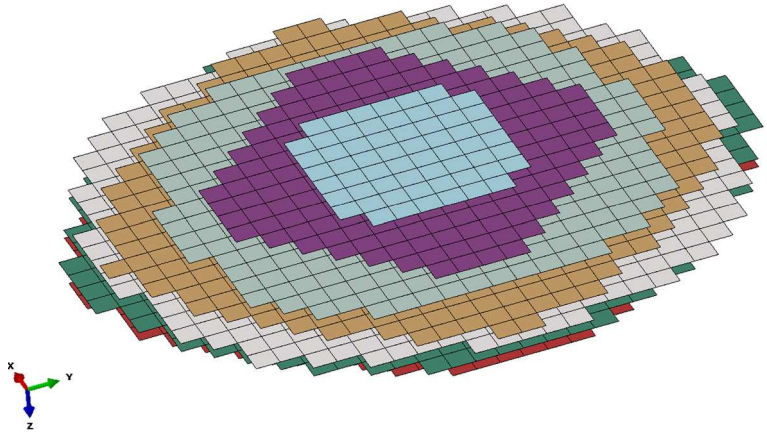

Fig. 9 Final delaminated elements for the structural model

material in term of volume fraction, $V_{Coh} = 0.24\,\%$ is very low with regard to the proportion of the RTM6 material $V_{Matrix} \approx 40\,\%$ which represents the matrix.

3.3 Models Comparison and Validation

As presented earlier, both models differ in their numerical results, while they present some similarities concerning the global behaviour of the specimen during the impact. In fact, both approaches are quite different, and the physical model presents a more realistic approach to the problem. In order to demonstrate the accuracy of both models, a comparison with the

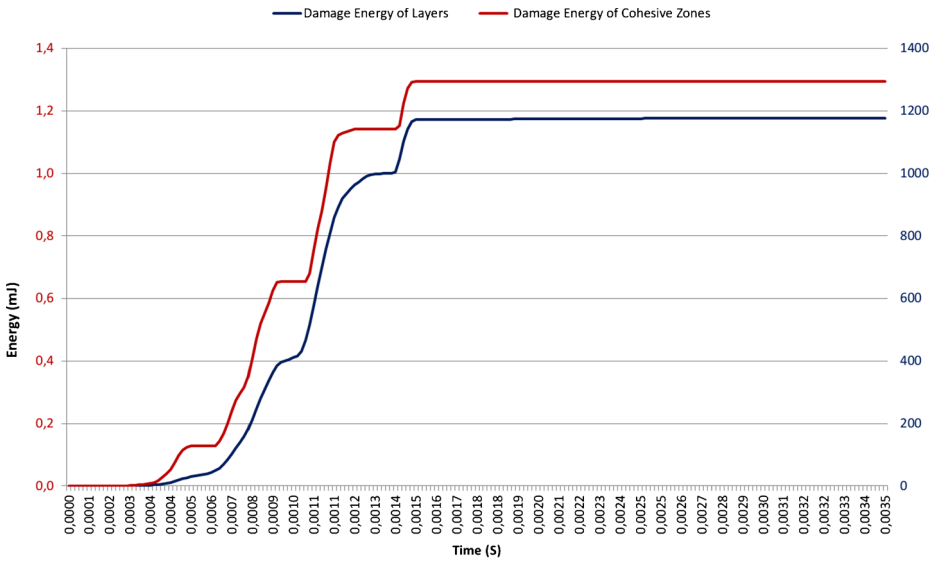

Fig. 10 Damage energies variation in cohesive zone and layers

experimental results presented in Section 2.2 is given here after. A comparison of the computed damaged surfaces obtained with the numerical models and the experimental results presented in Section 2.2 shows that both models are in accordance. In fact, the experimentally measured damaged surface given in the previous section is more or less the minimal value because of the technology used for this investigation. This is not an absolute value because of the experimental protocol and the measurement errors. In fact, the difference given by both simulations can be considered inside of the error measurement.

Roughly speaking, the use of the structural model gives a lot of satisfaction because, on the one hand, the numerical results are quite good and on the other hand, the amount of work requested to set-up the model is limited because of its simplicity. Concerning the physical model, the amount of work to set-up the model is larger than the one for the structural model, but on the other hand, this model is able to deliver more informations concerning the geometry and the evolution of the damaged zone with time. The structural model is a quite simple and robust approach, giving relatively accurate results for the proposed application. The computational cost is very low and this kind of model is very useful for dimensioning the structure. But, on the other hand, this kind of approach doesn't allow taking into account some very important points for composite structures such as transverse delamination for example. The physical model allows taking into account this transverse delamination as it is physically included in the model proposed. Of course, one must identify the mechanical behaviour of the matrix and the cohesive damage initiation and propagation parameters in order to obtain accurate results, which needs more experiments. Computational cost is also greater with regard to the structural model, but the model is able to give more precise results such as delamination and interfacial ruptures. All phenomena occurring in composite structures such as traction and compression damage of both layer and matrix can be computed using this approach.

4 Conclusions and Future Developments

The first part of this paper concern a bibliographic study of the degradation of composite structures subjected to BVID. The BVID have been identified in terms of energy and damages, and as a consequence the experimental device used for testing and validation has been set-up. Two major degradations process have been selected and developed: the layer damage and the cohesive interfacial damage models. On those assumptions, two finite element models have been developed: a structural model consisting in a global homogenized approach of the problem and a physical model consisting in a precise description of the composite structure taking into account all the layers of the specimen. Numerical results have shown that the structural model allows obtaining quite accurate results concerning the size of the damaged area with regard to the Hashin damage criterion used in the model in a limited computational time within a relatively simple approach. Cohesive interfaces behaviour introduced in the physical model with the help of the Benzegaggh-Kenane criterion leads to a more sophisticated approach able to deliver more fine results such as the delamination of the layers and the three-dimensional geometry of the damaged volume resulting from the impact solicitation. Both results are in accordance with the experiments and can be considered as a first step in this kind of work.

Acknowledgments The authors want to thanks the Daher Socata industry in Tarbes for having financial supporting this research.

References

1. Kaddour, A.S., Hinton, M.J., Smith, P.A., Li, S.: A comparison between the predictive capability of matrix cracking, damage and failure criteria for fibre reinforced composite laminates: Part a of the third world-wide failure exercise. J. Compos. Mater. **47**(20–21), 2749–2779 (2013)
2. Abrate, S.: Impact on laminated composite materials. Appl. Mech. Rev. **44**, 155–190 (1991)
3. Chai, P., Manikandan, G.B.: Low velocity impact response of fibre-metal laminates–a review. Compos. Struct. **107**, 363–381 (2014)
4. Burke, S.K., McKcousland, S., Scala, C.M.: Nondestructive characterization of advanced composite materials. Mater. Forum **18**, 85–109 (1994)
5. Garnier, C., Pastor, M.L., Eyma, F., Lorrain, B.: The detection of aeronautical defects in situ on composite structures using non destructive testing. Compos. Struct. **93**(5), 1328–1336 (2011)
6. Pastor, M.L., Garnier, C., Pescay, C.: Comparison of two nondestructive tests in carbon/epoxy composites. J. Mater. Sci. Eng. **4**(10), 14–20 (2009)
7. Garnier, C., Lorrain, B., Pastor, M.L.: Impact damage evolution under fatigue loading by infrared thermography on composite structures. In: International Conference on Experimental Mechanics (ICEM 14) (2010)
8. Hongkarnjanakul, N.: Modélisation numérique pour la tolérance aux dommages d'impact sur stratifié composite: de l'impact à la résistance résiduelle en compression. PhD thesis, Toulouse, ISAE (2013)
9. Olsson, R.: Mass criterion for wave controlled impact response of composite plates. Compos. A: Appl. Sci. Manuf. **31**(8), 879–887 (2000)
10. Sjöblom, P.O., Hartness, J.T., Cordell, T.M.: On low-velocity impact testing of composite materials. J. Compos. Mater. **22**, 30–52 (1988)
11. Shivakumar, K.N., Elber, W., Illg, W.: Prediction of low-velocity impact damage on thin circular laminates. J. Am. Inst. Aeronaut. Astronaut. **23**, 442–449 (1985)
12. Cantwell, W.J., Morton, J.: The impact resistance of composite materials - a review. Composites **22**, 347–362 (1991)
13. Liu, D., Malvern, L.E.: Matrix cracking in impacted glass/epoxy plates. J. Compos. Mater. **21**, 594–609 (1987)
14. Joshi, S.P.: Impact-induced fracture initiation and detailed dynamic stress field in the vicinity of impact. In: American Society of Composite 2nd Technical Conference (1987)
15. Cesari, F., Dal Re, V., Minak, G., Zuccheli, A.: Damage and residual strength of laminated carbon/epoxy composite circular plates loaded at the centre. Compos. Part A **38**, 1163–1173 (2007)
16. Allix, O., Ladevèze, P.: Interlaminar interface modelling for the prediction of laminates delamination. Compos. Struct. **22**, 235–242 (1992)
17. Kachanov, M.: Time of rupture process under creep conditions. Isv. Akad. Nauk. SSR. Otd Tekh. Nauk **8**, 26–31 (1958)
18. Rabotnov, Y.N.: Creep rupture. In: Proceedings XII, International Congress of Applied Mechanics (1968)
19. Hashin, Z.: Failure criteria for unidirectional fiber composites. J. Appl. Mech. **47**, 329–334 (1980)
20. Hashin, Z., Rotem, A.: A fatigue criterion for fiber-reinforced materials. J. Compos. Mater. **7**, 448–464 (1973)
21. Camanho, P.P., Dàvila, C.G.: Mixed-mode decohesion finite elements for the simulation of delamination in composite materials. Technical report, NASA TM-2002-211737 (2002)
22. Jäger, S., Pickett, A., Middendorf, P.: A discrete model for simulation of composites plate impact including coupled intra- and inter-ply failure. Appl. Compos. Mater. (2016)
23. Benzeggagh, M.L., Kenane, M.: Measurement of mixed-mode delamination fracture toughness of unidirectional glass/epoxy composites with mixed-mode bending apparatus. Composite Science and Technology **56**, 439–449 (1996)
24. Simulia, D.S.: The Abaqus v6.14 Documentation Collection (2014)
25. Ren, N., Ou, J.: Dynamic numerical simulation for ship-owt collision. In: 8th International Conference on Reliability, Maintainability and Safety, 2009. ICRMS 2009, pp. 1003–1007